Electronic Suplementary Information

0 Covariant expressions for the normalized directions of the Maxwell fields

Using the procedure described in the main text, we find from the Maxwell equations:

$$\boldsymbol{\nabla}\cdot\boldsymbol{D}=0, \qquad \boldsymbol{\nabla}\times\boldsymbol{E}=-\frac{\partial\boldsymbol{B}}{\partial t},$$

$$\boldsymbol{\nabla}\cdot\boldsymbol{B}=0, \qquad \boldsymbol{\nabla}\times\boldsymbol{B}=\mu_0\frac{\partial\boldsymbol{D}}{\partial t},$$

the following expressions for the normalized directions of the Maxwell fields associated with the extraordinary mode:

$$\boldsymbol{u}_b^{(e)}=\frac{\boldsymbol{p}^{(e)}\times\boldsymbol{n}}{\sqrt{\left|\boldsymbol{p}^{(e)}\right|^2-\left[\boldsymbol{n}\cdot\boldsymbol{p}^{(e)}\right]^2}},$$

$$\boldsymbol{u}_d^{(e)}=\frac{\left|\boldsymbol{p}^{(e)}\right|^2\boldsymbol{n}-\left[\boldsymbol{n}\cdot\boldsymbol{p}^{(e)}\right]\boldsymbol{p}^{(e)}}{\left|\boldsymbol{p}^{(e)}\right|\sqrt{\left|\boldsymbol{p}^{(e)}\right|^2-\left[\boldsymbol{n}\cdot\boldsymbol{p}^{(e)}\right]^2}},$$

$$\boldsymbol{u}_e^{(e)}=\sqrt{\epsilon^{(e)}}\,\frac{\epsilon_\perp\boldsymbol{n}-\left[\boldsymbol{n}\cdot\boldsymbol{p}^{(e)}\right]\boldsymbol{p}^{(e)}}{\epsilon_\perp\sqrt{\left|\boldsymbol{p}^{(e)}\right|^2-\left[\boldsymbol{n}\cdot\boldsymbol{p}^{(e)}\right]^2}},$$

$$\boldsymbol{u}_s^{(e)}=\sqrt{\epsilon^{(e)}}\,\frac{\epsilon_\perp\boldsymbol{p}^{(e)}+\epsilon_a\left[\boldsymbol{n}\cdot\boldsymbol{p}^{(e)}\right]\boldsymbol{n}}{\epsilon_\parallel\epsilon_\perp},$$

and the following expressions for the ordinary mode:

$$\boldsymbol{u}_b^{(o)}=\frac{\epsilon^{(o)}\boldsymbol{n}-\left[\boldsymbol{n}\cdot\boldsymbol{p}^{(o)}\right]\boldsymbol{p}^{(o)}}{\sqrt{\epsilon^{(o)}\left(\epsilon^{(o)}-\left[\boldsymbol{n}\cdot\boldsymbol{p}^{(o)}\right]^2\right)}},$$

$$\boldsymbol{u}_d^{(o)}=\frac{\boldsymbol{n}\times\boldsymbol{p}^{(o)}}{\sqrt{\epsilon^{(o)}-\left[\boldsymbol{n}\cdot\boldsymbol{p}^{(o)}\right]^2}},$$

$$\boldsymbol{u}_e^{(o)}=\boldsymbol{u}_d^{(o)},$$

$$\boldsymbol{u}_s^{(o)}=\frac{\boldsymbol{p}^{(o)}}{\sqrt{\epsilon^{(o)}}}.$$

Note that in these equations, we introduced the effective relative permittivity along the propagation axis $\epsilon^{(\alpha)}\equiv\left[\boldsymbol{p}^{(\alpha)}\cdot\boldsymbol{u}_s^{(\alpha)}\right]^2$ for the extraordinary ($\alpha=e$) and ordinary ($\alpha=o$) modes. The expressions of these effective relative permittivities are $\epsilon^{(o)}\equiv\epsilon_\perp$ and:

$$\epsilon^{(e)}=\frac{\epsilon_\parallel\epsilon_\perp^2}{\epsilon_\perp^2+\epsilon_a\left[\boldsymbol{n}\cdot\boldsymbol{p}^{(e)}\right]^2}.$$

1 Derivation of the Hamiltonian ray-tracing equations from the Fermat-Grandjean principle

A ray is defined as an integral curve of the vector field $\boldsymbol{u}_s^{(e)}$ or $\boldsymbol{u}_s^{(o)}$ – the direction in which the light "flows", since these vector fields correspond to the renormalised Poynting vector field. In a birefringent medium, each extraordinary ray $C^{(e)}$ or ordinary ray $C^{(o)}$ is submitted to the so-called Fermat-Grandjean principle[1] (strictly speaking it is a theorem, since it can be proven[2]):

$$\Delta\psi^{(\alpha)}\equiv\int_{C^{(\alpha)}}\boldsymbol{p}^{(\alpha)}\cdot\mathrm{d}\boldsymbol{r}^{(\alpha)}\text{ is extremal, with }\alpha=e\text{ or }o. \tag{1}$$

By definition of a ray, $\mathrm{d}\boldsymbol{r}^{(\alpha)}=\boldsymbol{u}_s^{(\alpha)}\mathrm{d}s$, where s is the arclength along the curve $C^{(\alpha)}$ (for simplicity sake, we don't use an index $\alpha=e$ or o on s since it can easily be inferred from the other terms in any equation). Using this observation and the results of Sec. 2.1 in the main text, it is easy to show that the Fermat-Grandjean principle (1) is equivalent to the following optimisation problem:

$$\boldsymbol{r}^{(\alpha)}=\mathrm{argmin}_{\boldsymbol{r}}\;\Delta\psi^{(\alpha)}[\boldsymbol{r}],\qquad\alpha=e\text{ or }o, \tag{2}$$

where we interpreted $\Delta\psi^{(e)}$ and $\Delta\psi^{(o)}$ as effective actions:

$$\Delta\psi^{(\alpha)}[\boldsymbol{r}]\equiv\int\mathcal{L}^{(\alpha)}\left(\boldsymbol{r},\frac{\mathrm{d}\boldsymbol{r}}{\mathrm{d}s}\right)\mathrm{d}s,\qquad\alpha=e\text{ or }o,$$

associated with the following Lagrangians for the extraordinary and ordinary rays:

$$\mathcal{L}^{(e)}\left(\boldsymbol{r},\frac{\mathrm{d}\boldsymbol{r}}{\mathrm{d}s}\right)=\sqrt{\epsilon_\parallel\left|\frac{\mathrm{d}\boldsymbol{r}}{\mathrm{d}s}\right|^2-\epsilon_a\left[\boldsymbol{n}(\boldsymbol{r})\cdot\frac{\mathrm{d}\boldsymbol{r}}{\mathrm{d}s}\right]^2},$$

$$\mathcal{L}^{(o)}\left(\boldsymbol{r},\frac{\mathrm{d}\boldsymbol{r}}{\mathrm{d}s}\right)=\sqrt{\epsilon_\perp\left|\frac{\mathrm{d}\boldsymbol{r}}{\mathrm{d}s}\right|^2}.$$

Note that along a physical ray (for which $\mathrm{d}\boldsymbol{r}/\mathrm{d}s$ is equal to $\boldsymbol{u}_s^{(e)}$ or $\boldsymbol{u}_s^{(o)}$ depending on the type of ray), it is easy to show that $\mathcal{L}^{(\alpha)}=\sqrt{\epsilon^{(\alpha)}}$, where the effective permittivities $\epsilon^{(\alpha)}$ ($\alpha=e$ or o) are defined in Sec. 2.1 of the main text. We also recall that the solution of the optimisation problem (1) is given by solving the Euler-Lagrange equations associated with $\mathcal{L}^{(\alpha)}$:

$$\frac{\delta\mathcal{L}^{(\alpha)}}{\delta\boldsymbol{r}}\equiv\frac{\partial\mathcal{L}^{(\alpha)}}{\partial\boldsymbol{r}}-\frac{\mathrm{d}}{\mathrm{d}s}\left[\frac{\partial\mathcal{L}^{(\alpha)}}{\partial\left(\frac{\mathrm{d}\boldsymbol{r}}{\mathrm{d}s}\right)}\right]=0,\qquad\alpha=e\text{ or }o. \tag{3}$$

We now want to obtain the equivalent Hamiltonian formulation of these equations. The Lagrangians $\mathcal{L}^{(e)}$ and $\mathcal{L}^{(o)}$ are homogeneous of degree 1 in $\mathrm{d}\boldsymbol{r}/\mathrm{d}s$, and therefore cannot be hyperregular – that is to say, the Legendre transformation allowing to switch to

a Hamiltonian formulation is ill-defined. To overcome this difficulty, we introduce the following regularised Lagrangians homogeneous of degree 2 in $\mathrm{d}\boldsymbol{r}/\mathrm{d}u$:

$$\bar{\mathcal{L}}^{(\alpha)}\left(\boldsymbol{r},\frac{\mathrm{d}\boldsymbol{r}}{\mathrm{d}\bar{s}}\right)=\frac{1}{2}\left[\mathcal{L}^{(\alpha)}\left(\boldsymbol{r},\frac{\mathrm{d}\boldsymbol{r}}{\mathrm{d}\bar{s}}\frac{\mathrm{d}\bar{s}}{\mathrm{d}s}\right)\frac{\mathrm{d}s}{\mathrm{d}\bar{s}}\right]^2,\qquad \alpha=e \text{ or } o,$$

with $\bar{s}$ a new (arbitrary for now) parametrisation. For this new formulation to be equivalent with the previous one, we need to show that the Euler-Lagrange equations associated with $\bar{\mathcal{L}}^{(e)}$ and $\bar{\mathcal{L}}^{(o)}$ are verified. A direct calculation gives:

$$\begin{aligned}\frac{\delta\bar{\mathcal{L}}^{(\alpha)}}{\delta\boldsymbol{r}}&\equiv\frac{\partial\bar{\mathcal{L}}^{(\alpha)}}{\partial\boldsymbol{r}}-\frac{\mathrm{d}}{\mathrm{d}\bar{s}}\left[\frac{\partial\bar{\mathcal{L}}^{(\alpha)}}{\partial\left(\frac{\mathrm{d}\boldsymbol{r}}{\mathrm{d}\bar{s}}\right)}\right]\\&=\frac{\mathrm{d}s}{\mathrm{d}\bar{s}}\left\{m^{(\alpha)}\frac{\partial\mathcal{L}^{(\alpha)}}{\partial\boldsymbol{r}}-\frac{\mathrm{d}}{\mathrm{d}s}\left[m^{(\alpha)}\frac{\partial\mathcal{L}^{(\alpha)}}{\partial\left(\frac{\mathrm{d}\boldsymbol{r}}{\mathrm{d}\bar{s}}\right)}\right]\right\},\end{aligned}$$

with $m^{(\alpha)}\equiv(\mathrm{d}s/\mathrm{d}\bar{s})\mathcal{L}^{(\alpha)}$ and $\alpha=e$ or o. Therefore, if we impose that the new parametrisation verifies $\mathrm{d}\bar{s}=\mathcal{L}^{(\alpha)}\mathrm{d}s$ (in which case $m^{(\alpha)}=1$), we find using the last equation and eqn 3:

$$\frac{\delta\bar{\mathcal{L}}^{(\alpha)}}{\delta\boldsymbol{r}}\equiv\frac{\partial\bar{\mathcal{L}}^{(\alpha)}}{\partial\boldsymbol{r}}-\frac{\mathrm{d}}{\mathrm{d}\bar{s}}\left[\frac{\partial\bar{\mathcal{L}}^{(\alpha)}}{\partial\left(\frac{\mathrm{d}\boldsymbol{r}}{\mathrm{d}\bar{s}}\right)}\right]=0,\qquad \alpha=e \text{ or } o,$$

i.e. the Euler-Lagrange equations associated with $\bar{\mathcal{L}}^{(e)}$ and $\bar{\mathcal{L}}^{(o)}$ are verified. Note that since we imposed $\mathrm{d}\bar{s}=\mathcal{L}^{(\alpha)}\mathrm{d}s$, $\bar{s}$ can be directly identified with $\Delta\psi^{(\alpha)}$ with $\alpha=e$ or o depending on the type of ray, i.e. $\bar{s}$ can be identified with the optical length (defined as the arclength times the averaged effective index along the ray).

We can finally switch to the Hamiltonian formulation by computing the following Legendre transformation:

$$\mathcal{H}^{(\alpha)}=\boldsymbol{p}\cdot\frac{\mathrm{d}\boldsymbol{r}}{\mathrm{d}\bar{s}}-\bar{\mathcal{L}}^{(\alpha)},$$

with $\boldsymbol{p}\equiv\partial\bar{\mathcal{L}}^{(\alpha)}/\partial\left(\mathrm{d}\boldsymbol{r}/\mathrm{d}\bar{s}\right)$ the conjugate momentum. After some simplifications, we then obtain the following expressions for the Hamiltonians associated with the extraordinary and ordinary rays:

$$\mathcal{H}^{(e)}(\boldsymbol{r},\boldsymbol{p})=\frac{\epsilon_\perp|\boldsymbol{p}|^2+\epsilon_a\left[\boldsymbol{n}(\boldsymbol{r})\cdot\boldsymbol{p}\right]^2}{2\epsilon_\parallel\epsilon_\perp},$$

$$\mathcal{H}^{(o)}(\boldsymbol{r},\boldsymbol{p})=\frac{|\boldsymbol{p}|^2}{2\epsilon_\perp},$$

The Hamilton equations associated with $\mathcal{H}^{(e)}$ and $\mathcal{H}^{(o)}$ are given in the main text.

2 Derivation of the transport equation for the geometrical spreadings

In this section, we explicit the proof of the transport equations for the geometrical spreadings $q^{(e)}$ and $q^{(o)}$. First, let us characterise the transport properties of $\mathbf{J}^{(e)}$ and $\mathbf{J}^{(o)}$ along rays. Starting from the definitions of these two quantities in the main text, we obtain:

$$\frac{\partial J_{ij}^{(\alpha)}}{\partial\bar{s}}=\frac{\partial v_i^{(\alpha)}}{\partial x_{0j}},$$

with $\boldsymbol{v}^{(\alpha)}\equiv\partial\boldsymbol{r}^{(\alpha)}/\partial\bar{s}=\boldsymbol{u}_s^{(\alpha)}/\sqrt{\epsilon^{(\alpha)}}$ and $\alpha=e$ or o. By switching from the Lagrangian formalism to the Eulerian formalism, we then find:

$$\frac{\mathrm{d}J_{ij}^{(\alpha)}}{\mathrm{d}\bar{s}}=\sum_k\frac{\partial v_i^{(\alpha)}}{\partial r_k}J_{kj}^{(\alpha)},$$

or equivalently:

$$\frac{\mathrm{d}\boldsymbol{J}^{(\alpha)}}{\mathrm{d}\bar{s}}=\left[\boldsymbol{\nabla}\boldsymbol{v}^{(\alpha)}\right]^{\mathsf{T}}\boldsymbol{J}^{(\alpha)},\qquad \alpha=e \text{ or } o. \tag{4}$$

Second, let us characterise the transport properties of $q^{(\alpha)}\equiv\det\left[\mathbf{J}^{(\alpha)}\right]$ along rays. By using the Jacobi formula for invertible matrices, we directly obtain:

$$\frac{\mathrm{d}q^{(\alpha)}}{\mathrm{d}\bar{s}}=q^{(\alpha)}\,\mathrm{Tr}\left\{\left[\boldsymbol{J}^{(\alpha)}\right]^{-1}\frac{\mathrm{d}\boldsymbol{J}^{(\alpha)}}{\mathrm{d}\bar{s}}\right\},\qquad \alpha=e \text{ or } o. \tag{5}$$

By combining eqn (4) and eqn (5) and using the similarity-invariance of the trace, we obtain:

$$\frac{\mathrm{d}q^{(\alpha)}}{\mathrm{d}\bar{s}}=q^{(\alpha)}\,\mathrm{Tr}\left\{\left[\boldsymbol{\nabla}\boldsymbol{v}^{(\alpha)}\right]^{\mathsf{T}}\right\},$$

or equivalently:

$$\frac{\mathrm{d}q^{(\alpha)}}{\mathrm{d}\bar{s}}=q^{(\alpha)}\left(\boldsymbol{\nabla}\cdot\boldsymbol{v}^{(\alpha)}\right),\qquad \alpha=e \text{ or } o.$$

The last equation is equivalent to the two transport equations for the geometrical spreadings given in the main text after using the definitions of $\boldsymbol{v}^{(e)}$ and $\boldsymbol{v}^{(o)}$.

3 Description of the steps involved in our ray-tracing algorithm

For convenience, we reproduce here the figure of the main text describing the two birefringent systems supported by our algorithm (Fig. 1) as well as the general iterative procedure used in our numerical code:

(A1) Initial setup of the rays on the source plane; the target plane is initially aligned with the source plane.

(A2) While the target plane has not reached the end of the sample, do the following steps:

- (A2.1) Move the target plane with a small vertical increment and propagate the rays until they cross the new position of the target plane.
- (A2.2) Reconstruct the electric and magnetic field at the new end points of the rays.
- (A2.3) Interpolate the values of the electric and magnetic field on the regular grid associated with the target plane.

In the next subsections, we detail the steps (A1), (A2.1), (A2.2) and (A2.3) of this algorithm.

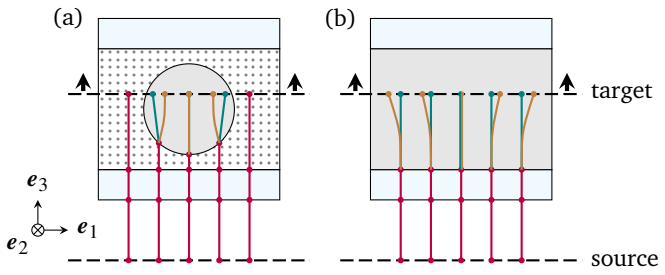

Fig. 1 The numerical implementation of our improved ray-tracing method consider two types of system in which light is propagated: (a) birefringent droplet (gray color) in suspension in an isotropic medium (dotted domain) or (b) slab of constant thickness of a birefringent medium (gray color again). In both cases, two parallel isotropic plates (blue rectangles) are used to contain the sample. We assume that the incident light is a plane wave, in which case the hypersurface defining the light source is just a reference plane below the sample. Rays (in red if isotropic, in green if ordinary, in brown if extraordinary) are propagated in the sample by pushing upward a target plane containing the end points of the rays. Special care is taken when a surface of discontinuity of the optical index is encountered, as explained in the main text.

3.1 Setup of the source and target planes (step A1)

Since we assumed that the light source is a plane wave incident normally on the sample, the renormalized wave vector for any incident ray is $\boldsymbol{p}_i = n_i \boldsymbol{e}_3$, with n_i the optical index of the incident medium and $\boldsymbol{e}_3$ the unit vector defining the upward direction (see Fig. 1). We can therefore choose any plane orthogonal to $\boldsymbol{e}_3$ for the reference surface defining the light source, as long as this plane is below the sample. We will assume that the origin of the $\boldsymbol{e}_3$ is aligned with this plane.

Next, we define on the source plane a regular grid of "seed" points from which the rays will "grow". The points of this grid are defined with the following formula:

$$\boldsymbol{x}_s(i_1,i_2) = \boldsymbol{q}_s + i_1\, a_1\, \boldsymbol{e}_1 + i_2\, a_2\, \boldsymbol{e}_2, \quad i_{1,2} = 0 \ldots N_{1,2} - 1.$$

In this formula, $\boldsymbol{q}_s$ is the origin of the grid, a_1 and a_2 are the cell widths, and $N_{1,2}$ are the number of points in each directions. The unit vectors $\boldsymbol{e}_1$ and $\boldsymbol{e}_2$ are defined on Fig. 1.

The target plane is initially aligned with the source plane, and will be moved along the $\boldsymbol{e}_3$ axis in the later stages of our algorithm. The vertical shift between the source and target planes will be denoted by z. Similarly to the source plane, we also define on the target plane a regular grid of points on which we will interpolate the electric and magnetic fields. The points $\boldsymbol{x}_t$ of this grid are defined similarly to the seed points of the source plane:

$$\boldsymbol{x}_t(i_1,i_2) = \boldsymbol{q}_t + i_1\, a'_1\, \boldsymbol{e}_1 + i_2\, a'_2\, \boldsymbol{e}_2, \quad i_{1,2} = 0 \ldots N'_{1,2} - 1.$$

Note that instead of initializing a single ray at each seed point $\boldsymbol{x}_s(i_1,i_2)$ of the regular grid, we initialize what we call a *ray bundle*, consisting of a primary ray emanating from $\boldsymbol{x}_s(i_1,i_2)$ and three shifted secondary rays whose starting points are $\boldsymbol{x}_s(i_1,i_2) + \mu\, \boldsymbol{e}_j$ ($j = 1,2,3$), with $\mu \ll a_{1,2}$. These four rays will be propagated in parallel using the ray-tracing equations, with the additional constraint that the optical length associated with these four rays are the same. As we will see in a moment, this strategy will allow us to easily estimate the geometrical spreading associated with each ray bundle.

At any point in our algorithm, the current state of a ray bundle is represented by the values of the following quantities (evaluated at the current end point of the ray bundle):

1. The positions of the primary and secondary rays
2. The momenta of the primary and secondary rays
3. The polarisation vectors
4. The eikonal function
5. The electric field amplitude

Since we start from a plane wave, we can assume that initially, the eikonal function is zero and the electric field amplitude is constant. The initial polarisation state must be specified on the light source.

3.2 Update of the target plane and rays (step A2.1)

The first step in the main propagation loop of our algorithm is to shift upward the target plane with a small increment $a_3 \boldsymbol{e_3}$. In each ray bundle, the primary ray is propagated forward until it crosses the new position of the target plane and the secondary rays are propagated forward until they have the same optical length as the primary ray.

If the considered ray is in the birefringent medium, we use the ray-tracing equations of Sec. 2.2 of the main text. These ordinary differential equations are solved using a first-order predictor-corrector scheme with adaptive control of the integration step. In this scheme, the predictor step is simply an explicit Euler step and the corrector step consists in renormalising the amplitude of the momentum in order to preserve the value of the Hamiltonian. Since this scheme is not simplectic (but considerably simpler to implement because it is explicit), the integration step is adjusted until the Hamiltonian variation during the predictor step is lower than a user-defined threshold value.

If the considered ray is in an isotropic domain, we use the isotropic limit of the previous ray-tracing equations ($\epsilon_\parallel = \epsilon_\perp = [n_r]^2$ with n_r the optical index of the considered isotropic domain). It can be directly checked that the solutions of these equations are straight lines in this limit, which means that we can rely on fully analytical formula to propagate rays inside isotropic media.

Special care must be taken if a ray crosses a surface of discontinuity of the optical index since most of the quantities defining the state of a ray bundle are discontinuous at such an interface. Here, we closely follow the approach of Sluijter et al.[3] by using the general Fresnel boundary conditions. These boundary conditions allow us to compute the new state of the ray bundles from the continuity conditions on the tangential components of $\boldsymbol{p}$, $\boldsymbol{E}$ and $\boldsymbol{H}$. At any interface of discontinuity, an incident ray will produce in general 1 or 2 reflected rays (1 if the incidence medium is isotropic, else 2) and 1 or 2 transmitted rays (1 if the transmission medium is isotropic, else 2). In our code, we neglect multiple

reflections and propagate forward only transmitted rays. This approximation is valid as long as the typical jump of permittivity between the different media is small.

Since we consider only one convex birefringent medium enclosed by isotropic media, only one ray-splitting {*isotropic ray* → *extraordinary + ordinary ray*} can occur in the sample. This allows us to define the following families of rays: isotropic rays which never encountered the birefringent medium (red lines in Fig. 1), and extraordinary/ordinary rays (brown and green lines in Fig. 1) coming from the birefringent medium. We denote the last two families of rays with an (e) or (o) index as in the main text, and the family of isotropic rays with an (i) index.

3.3 Reconstruction of the Maxwell fields (step A2.2)

Once the trajectories of the rays are updated, one can directly compute the new values of the polarisation vectors using the results of Sec. 2.1 in the main text. The polarisation of the isotropic rays stays unchanged since it can only change at surface of discontinuity of the optical index – which was taken care of in step (A2.1).

To reconstruct the electric field amplitude, we use the main result of Sec. 2.3 in the main text:

$$E^{(\alpha)} = \frac{\mathcal{F}^{(\alpha)}}{\sqrt{q^{(\alpha)}\epsilon^{(\alpha)}}}, \qquad \alpha = e,i \text{ or } o. \tag{6}$$

Note that in the main text, we only considered extraordinary and ordinary rays (index $(e)/(o)$), but the formula for the isotropic rays can be easily obtained by taking the isotropic limit ($\epsilon^{(i)} \equiv \epsilon_{\parallel} = \epsilon_{\perp} = [n_r]^2$). These equations requires the value of the geometrical spreading ($q^{(e)}$ and $q^{(e)}$ for extraordinary/ordinary rays and $q^{(i)}$ for isotropic rays). We obtain these quantity from the determinants of the Jacobian matrices $\mathbf{J}^{(\alpha)}$, which we compute using a finite-difference approximation:

$$J_{ij}^{(\alpha)} \approx \frac{r_i^{(\alpha)}\left(\bar{s}, \boldsymbol{x}_0 + \mu\, \boldsymbol{e}_j\right) - r_i^{(\alpha)}\left(\bar{s}, \boldsymbol{x}_0\right)}{\mu}. \qquad \alpha = e,i \text{ or } o. \tag{7}$$

Since we constrained that all rays in each ray bundle have the same optical length, the first (resp., second) term in the last equation can be directly evaluated using the current positions of the secondary rays (resp., the current position of the primary ray).

Once the amplitude, eikonal function, and polarisation are updated along an extraordinary, ordinary or isotropic ray bundle, the new value of the electric field along the same ray bundle is approximated by keeping only the zero-th order term in the WKB expansion:

$$\boldsymbol{E}^{(\alpha)} \approx E_0^{(\alpha)} \exp\left[ik_0\psi^{(\alpha)} - i\omega t\right] \boldsymbol{u}_e^{(\alpha)}, \qquad \alpha = e,i \text{ or } o.$$

The magnetic field is then obtained by keeping only the zero-th order term in the Maxwell-Faraday equation (see Sec. 2.1 in the main text):

$$\boldsymbol{B}^{(\alpha)} \approx \frac{\boldsymbol{p}^{(\alpha)} \times \boldsymbol{E}^{(\alpha)}}{c}, \qquad \alpha = e,i \text{ or } o.$$

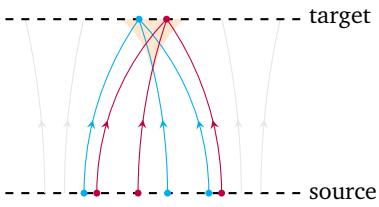

Fig. 2 When the deflection effect is strong, rays of the same family can cross with each other, as represented in this figure. In the white domain, there is a one-to-one correspondence between points of this domain and source points on the reference plane. In the red domain (where rays are crossing with each other), each target point is associated with three possible source points, as illustrated with the blue and red rays.

3.4 Interpolation of the Maxwell fields (step A2.3)

Since there are several families of ray (isotropic, extraordinary and ordinary), we need to recombine the Maxwell fields associated with each family to obtain the total electric and magnetic fields on the target plane. Furthermore, our reconstruction method only gives the electric and magnetic fields along the ray bundles, which means that interpolation is necessary to access the full electric and magnetic fields at the points $\boldsymbol{x}_t(i_1,i_2)$ on the target plane. This interpolation is not trivial to implement because the trajectories of the rays are curved and can even intersect with each other — in which case multiple values of $\boldsymbol{E}$ corresponding to different rays of the same family contribute to the local value of the electric field, see Fig. 2. Regions of space where rays of the same family are crossing with each other are called *caustic domains*. The boundaries of such domains are simply called *caustics*. These caustics often have a cusp singularity (as in Fig. 2), but more generic shapes are possible[4].

To accurately reconstruct the full electric and magnetic fields on the target plane, it is therefore of paramount importance to find for each target point every possible rays arriving at this point. Our strategy to do this is to formally construct for each ray family a C^1 mapping linking the source plane to the target plane:

$$\boldsymbol{\pi}^{(\alpha)} : \boldsymbol{x}_0 \to \boldsymbol{r}^{(\alpha)}\left(\bar{s}, \boldsymbol{x}_0\right), \qquad \alpha = e,i \text{ or } o,$$

where the optical length $\bar{s}$ is constrained so that $\boldsymbol{r}^{(\alpha)}\left(\bar{s}, \boldsymbol{x}_0\right)$ is on the target plane. These three mappings can be directly constructed using the current states of the ray bundles and bicubic interpolation (similarly to the tricubic interpolation algorithm associated with the $\boldsymbol{n}$ mapping, we generate the C code for the interpolation kernel using a symbolic calculation in Mathematica). Finding all rays arriving at a point $\boldsymbol{x}_t$ of the target plane is then equivalent to finding the sets $\mathcal{S}^{(\alpha)}(\boldsymbol{x}_t)$ ($\alpha = e,i$ or o) of source points defined by:

$$\mathcal{S}^{(\alpha)}(\boldsymbol{x}_t) \equiv \left\{\boldsymbol{x}_s \;\middle|\; \pi^{(\alpha)}(\boldsymbol{x}_s) = \boldsymbol{x}_t\right\}$$

Formally speaking, these sets corresponds to the preimages of the singleton set $\{\boldsymbol{x}_t\}$ under the mappings $\boldsymbol{\pi}^{(\alpha)}$. Numerically, we construct the sets $\mathcal{S}^{(\alpha)}(\boldsymbol{x}_t)$ using a homotopy continuation algorithm detailed in the next section.

Once these sets have been obtained for a target point $\boldsymbol{x}_t$, the electric and magnetic fields at $\boldsymbol{x}_t$ is simply obtained by summing

the contributions from all rays arriving at $\boldsymbol{x}_t$:

$$\boldsymbol{E}(\boldsymbol{x}_t) = \sum_{\alpha=e,i,o} \sum_{\boldsymbol{x}_s \in \mathcal{S}^{(\alpha)}(\boldsymbol{x}_t)} \boldsymbol{E}^{(\alpha)}(\boldsymbol{x}_s)$$

$$\boldsymbol{B}(\boldsymbol{x}_t) = \sum_{\alpha=e,i,o} \sum_{\boldsymbol{x}_s \in \mathcal{S}^{(\alpha)}(\boldsymbol{x}_t)} \boldsymbol{B}^{(\alpha)}(\boldsymbol{x}_s)$$

Again, the mappings $\boldsymbol{E}^{(\alpha)}(\boldsymbol{x}_0)$ and $\boldsymbol{B}^{(\alpha)}(\boldsymbol{x}_0)$ are constructed using the current states of the ray bundle and bicubic interpolation. The last two equations are applied for every target points $\boldsymbol{x}_t(i_1, i_2)$ of the regular grid associated with the target plane, which allows us to obtain the full electric and magnetic fields on the target plane.

4 Homotopy continuation algorithm

In this appendix, we show how to numerically construct the preimage sets $\mathcal{S}^{(\alpha)}(\boldsymbol{x}_t)$ with $\alpha = e, i$ or o. Constructing these sets is mathematically equivalent to finding all zeros of a function $\boldsymbol{f} : \mathbb{R}^2 \to \mathbb{R}^2$ defined by:

$$\boldsymbol{f}(\boldsymbol{x}_s) = \boldsymbol{\pi}^{(\alpha)}(\boldsymbol{x}_s) - \boldsymbol{x}_t,$$

with $\alpha = e, i$ or o. In the following discussion, we forget about the (e)/(i)/(o) index and focus on finding the zeros of the function $\boldsymbol{f}$.

The most basic strategy that can be tried to find a zero of $\boldsymbol{f}$ is to apply the Newton algorithm. This strategy has two problems: it is not globally convergent (i.e. we are not sure to converge to a zero of $\boldsymbol{f}$), and even if a zero is found, it is difficult to find other solutions. A much better alternative is to use a homotopy continuation algorithm. The basic idea behind homotopy continuation is to "extend" the function $\boldsymbol{f}(\boldsymbol{x})$ in a new function $\boldsymbol{h}(\boldsymbol{x}, \beta)$ using a continuous parameter β. The extended function must verify two properties:

1. The function $\boldsymbol{h}(\boldsymbol{x}, 0)$ must have a trivial zero (i.e. a zero which can be analytically found).
2. The function $\boldsymbol{h}(\boldsymbol{x}, 1,)$ must be equal to $\boldsymbol{f}(\boldsymbol{x})$.

Then, zeros of the function $\boldsymbol{f}$ can be found by tracking the curve $\{\boldsymbol{x}(s), \beta(s)\}$ defined by $\boldsymbol{h}(\boldsymbol{x}(s), \beta(s)) = \boldsymbol{0}$ (with s the arclength of this 3D curve). A starting point for this curve can be trivially found on the hyperplane $\beta = 0$ (property 1 above), and each time this curve cross the hyperplane $\beta = 1$, we can record a new zero of the function $\boldsymbol{f}$ (property 2 above).

Several choices are possible for the extended function $\boldsymbol{h}$, the most common being the fixed-point homotopy function:

$$\boldsymbol{h}_{\mathrm{FP}}(\boldsymbol{x}, \beta) = \beta\, \boldsymbol{f}(\boldsymbol{x}) + (1 - \beta)(\boldsymbol{x} - \boldsymbol{x}_0) \tag{8}$$

and the Newton homotopy function:

$$\boldsymbol{h}_{\mathrm{N}}(\boldsymbol{x}, \beta) = \beta\, \boldsymbol{f}(\boldsymbol{x}) + (1 - \beta)\, [\boldsymbol{f}(\boldsymbol{x}) - \boldsymbol{f}(\boldsymbol{x}_0)] \tag{9}$$

In both cases, the starting point on the hyperplane $\beta = 0$ is the user-defined point $\boldsymbol{x}_0$. Even if these choices of extended function do not always lead to global convergence, they are typically far more robust than the basic Newton algorithm[5]. However, finding multiple zeros is still a challenge because it is absolutely not obvious that the same homotopy path $\{\boldsymbol{x}(s), \beta(s)\}$ will include all roots of function $\boldsymbol{f}$: in many cases, some roots are included in disconnected paths which do not cross the starting point $\boldsymbol{x}_0$ on the hyperplane $\beta = 0$ (see Fig. 3a and Fig. 3b for a 1D example).

A possibility to address this challenge is to introduce more complicated mapping for the extended function $\boldsymbol{h}$ (toroidal mapping, boomerang mapping...) in order to link together the disconnected homotopy paths[6]. Following the ideas of Seader *et al.*[6], we developed two new homotopy functions which empirically gave us very good results for the root finding problem. These two functions are the "trigonometric" fixed-point homotopy function:

$$\hat{\boldsymbol{h}}_{\mathrm{FP}}(\boldsymbol{x}, \beta) = \sin\left[\frac{\beta\pi}{2}\right] \boldsymbol{f}(\boldsymbol{x}) + \cos\left[\frac{\beta\pi}{2}\right] (\boldsymbol{x} - \boldsymbol{x}_0) \tag{10}$$

and the "trigonometric" Newton homotopy function:

$$\hat{\boldsymbol{h}}_{\mathrm{N}}(\boldsymbol{x}, \beta) = \sin\left[\frac{\beta\pi}{2}\right] \boldsymbol{f}(\boldsymbol{x}) + \cos\left[\frac{\beta\pi}{2}\right] [\boldsymbol{f}(\boldsymbol{x}) - \boldsymbol{f}(\boldsymbol{x}_0)]\,. \tag{11}$$

Instead of using a simple mapping linear in β as in eqn (8,9), these new homotopy functions use a trigonometric mapping which "fold" the homotopy axis β onto itself, thus forming a circle. This folding allows to connect more roots with the same homotopy path, as can be seen on Fig. 3c. Here, the roots are found each time the homotopy path $\{\boldsymbol{x}(s), \beta(s)\}$ crosses one of the hyperplane $\beta = \pm(2k + 1)$ (with k an integer), on which the function $\hat{\boldsymbol{h}}_{\mathrm{FP,N}}$ is equal to $\pm\boldsymbol{f}$. Since the homotopy function is 4-periodic in β, this is equivalent to recording the roots on the hyperplane $\beta = \pm 1$.

Numerically, the homotopy path $\{\boldsymbol{x}(s), \beta(s)\}$ verifying $\boldsymbol{h}(\boldsymbol{x}(s), \beta(s)) = \boldsymbol{0}$ can be obtained using the same class of predictor-corrector method described by Seydel[7]. Briefly, we use an arclength parametrisation for the homotopy curve $z(s) \equiv \{\boldsymbol{x}(s), \beta(s)\}$ to take into account possible turning points. At the n-th iteration of the algorithm, the current end position of the homotopy path z_n must verify $\boldsymbol{h}(z_n) = \boldsymbol{0}$ with $\boldsymbol{h}$ the chosen homotopy function. The next position is computed with the following formula:

$$z_{n+1} = z_n + \Delta z_p + \Delta z_c$$

Here, the predictor step Δz_p is proportional to the tangent vector of the curve $z(s)$ and the corrector step Δz_c (which is constrained to be in the hyperplane normal to Δz_p) is adjusted to impose $\boldsymbol{h}(z_{n+1}) = \boldsymbol{0}$.

Note that the findings of Choi and Book[8] also applies to our method: even with these complex choices of homotopy functions, it sometimes happens that a root is disconnected from the main homotopy path. This is of course quite natural, given the complexity of the problem that we want to solve (finding all roots of a non-transcendental function). But we empirically found that when the number of roots is low (typically ≤ 3), at least one the two homotopy functions $\hat{\boldsymbol{h}}_{\mathrm{FP,N}}$ is robust enough to reconstruct all the zeros of the function $\boldsymbol{f}$.

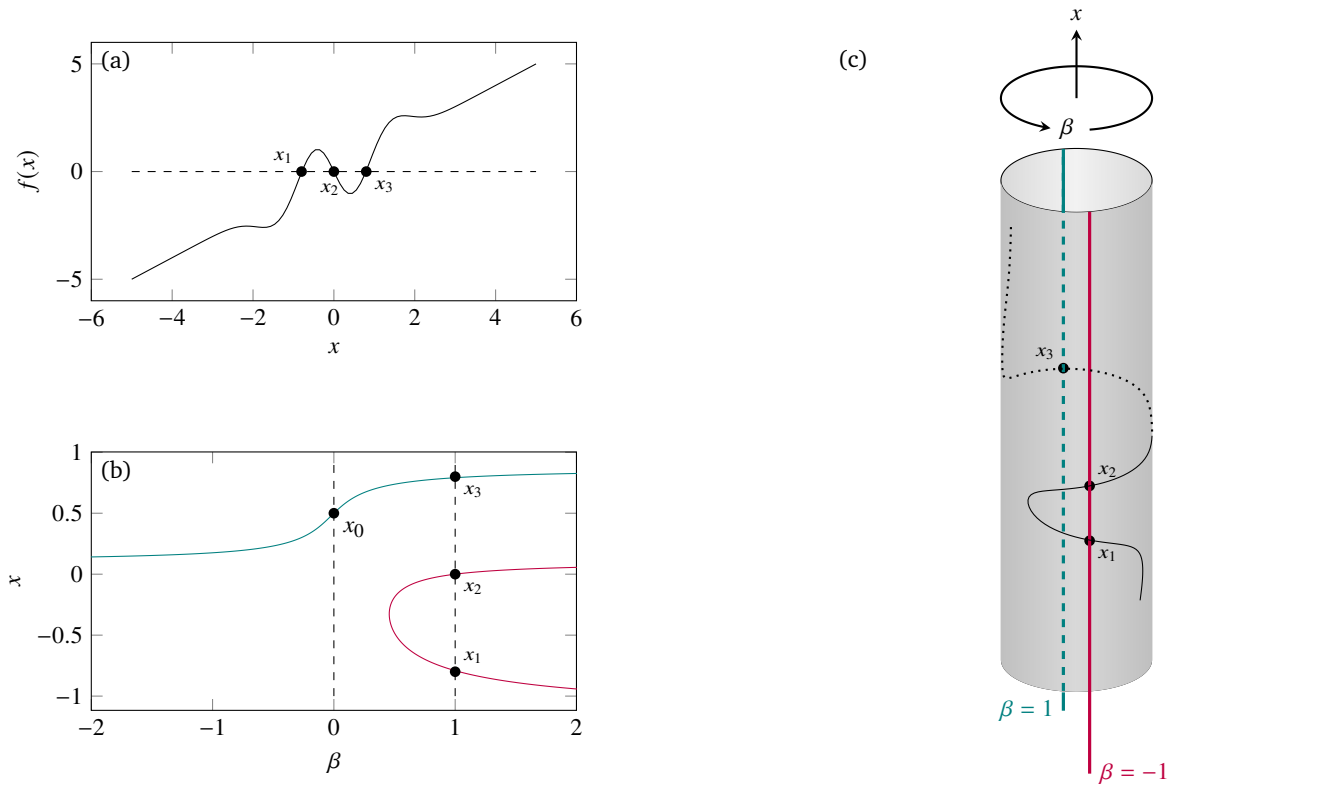

Fig. 3 (a) An example of a 1D function $f(x)$ associated with three roots x_1, x_2 and x_3. (b) Homotopy paths numerically obtained from the homotopy function h_{FP} (eqn (8)) associated with the function f of (a). The three roots $x_{1,2,3}$ are not contained in the same path starting at x_0. (c) Homotopy path numerically obtained from the homotopy function $\hat{h}_{\mathrm{FP}}$ (eqn (10)) associated with the function f of (a). This time the three roots are included in the same path. To underline the inherent periodicity of the homotopy function $\hat{h}_{\mathrm{FP}}$, the homotopy path is plotted on a cylinder, with the vertical coordinate corresponding to the x-axis and the orthoradial coordinate corresponding to the β-axis. Roots are obtained when the homotopy path crosses the $\beta = \pm 1$ lines.

5 Estimation of the starting point of the caustics

In this section, we estimate the vertical position z_c where caustics start developing in the system described in Sec. 3 of the main text. Instead of directly solving the ray-tracing equations, we use the Noether theorem to find the conserved quantities of the problem. We start from the director field associated with the system described in Sec. 3 of the main text:

$$\boldsymbol{n}(x,y,z) = \cos[qx]\,\boldsymbol{e}_y + \sin[qx]\,\boldsymbol{e}_z,$$

where $q = 2\pi/P$ is the spontaneous twist of the cholesteric phase. Since the only spatial dependence in the Hamiltonian associated with the extraordinary rays comes from the $\boldsymbol{n}(x,y,z)$ term (see Sec. 2.2 of the main text), the spatial symmetries of the Hamiltonian are the same as the spatial symmetries of the director field. Therefore, the translational invariance of the director field along the y and z axis implies that the y and z components of the moment $\boldsymbol{p}$ are conserved along a ray. By applying the Fresnel boundary conditions at the isotropic/cholesteric interface $z = 0$, we then deduce that $p_y = 0$ and:

$$p_z = \sqrt{\frac{\epsilon_\parallel \epsilon_\perp}{\epsilon_\perp + \epsilon_a \sin^2 qx_0}},$$

where x_0 is the initial x-coordinate for the considered ray. Moreover, the Hamiltonian does not explicitly depend on the ray parametrisation $\bar{s}$, from which we can deduce that the value of the Hamiltonian is conserved along a ray:

$$\mathcal{H}^{(e)} = \frac{p_x^2}{2\epsilon_\parallel} + \frac{\epsilon_\perp + \epsilon_a \sin^2 qx}{2\left(\epsilon_\perp + \epsilon_a \sin^2 qx_0\right)} = \frac{1}{2}$$

Using $\mathrm{d}x/\mathrm{d}\bar{s} = \partial\mathcal{H}^{(e)}/\partial p_x = p_x/\epsilon_\parallel$, we then arrive at the following implicit solution for the x-component $x(\bar{s}, x_0)$ of the extraordinary ray trajectory starting at x_0:

$$q\bar{s} = \sqrt{\epsilon_\parallel\left(\frac{\epsilon_\perp}{\epsilon_a} + \sin^2 q_0\right)} \int_{qx(\bar{s},x_0)}^{qx_0} \frac{\mathrm{d}u}{\sqrt{\sin^2 qx_0 - \sin^2 u}}$$

Using the change of variable $\sin v = \sin u/\kappa$ with $\kappa \equiv \sin qx_0$, the last equation can be expressed as a function of elliptic integrals:

$$q\bar{s} = \sqrt{\epsilon_\parallel\left(\frac{\epsilon_\perp}{\epsilon_a} + \kappa^2\right)} \left\{\mathrm{K}[\kappa] - \mathrm{F}\left[\arcsin\left(\frac{\sin qx\,[\bar{s}, x_0]}{\kappa}\right), \kappa^2\right]\right\}$$

where $\mathrm{K}(k)$ is the complete elliptic integral of the first kind and $\mathrm{F}(\phi, k)$ is the incomplete elliptic integral of the first kind.

The vertical position z_c where caustics start developing can be found by studying the set of rays which crosses with each other on the central z-axis. By setting $x = 0$ in the previous equation,

we find that two rays starting at $\pm x_0$ intersect with each other on the z-axis if and only if:

$$q\bar{s} = \sqrt{\epsilon_{\parallel}\left(\frac{\epsilon_{\perp}}{\epsilon_a} + \sin^2 qx_0\right)}\mathrm{K}(\sin^2 qx_0),$$

where the two rays have the same optical length $\bar{s}$ since they have symmetric trajectories with respect to the z-axis. By minimizing the previous equation with respect to x_0, we finally find the analytical expression of z_c:

$$z_c = \frac{\bar{s}_{\min}}{\sqrt{\epsilon_{\perp}}} = \frac{K(0)}{q}\sqrt{\frac{\epsilon_{\perp}}{\epsilon_a}} = \frac{P}{4}\sqrt{\frac{\epsilon_{\perp}}{\epsilon_{\parallel} - \epsilon_{\perp}}}.$$

Note that the last formula is only valid for positive birefringence. If the birefringence is negative, $\epsilon_{\parallel}$ and $\epsilon_{\perp}$ needs to be reversed in the last equation.

References

1 F. Grandjean, *Bulletin de la Société Française de Minéralogie*, 1919, **42**, 42.

2 P. Oswald and P. Pieranski, *Nematic and cholesteric liquid crystals: concepts and physical properties illustrated by experiments*, CRC press, 2006.

3 M. Sluijter, D. K. G. de Boer and J. J. M. Braat, *Journal of the Optical Society of America A*, 2008, **25**, 1260.

4 V. I. Arnold, S. M. Gusejn-Zade and A. N. Varčenko, *Singularities of differentiable maps. Vol. 1: The classification of critical points, caustics and wave fronts*, Birkhäuser, Boston, 1985.

5 T. Wayburn and J. Seader, *Computers & Chemical Engineering*, 1987, **11**, 7–25.

6 J. D. Seader, M. Kuno and J. W. Wiskin, *Computers & Chemical Engineering*, 1990, 15.

7 R. Seydel, *Practical bifurcation and stability analysis*, Springer Science & Business Media, 2009, vol. 5.

8 S. H. Choi and N. L. Book, *AIChE Journal*, 1991, **37**, 1093–1095.